Palaeogeography, Palaeoclimatology, Palaeoecology 626 (2023) 111702

Contents lists available at ScienceDirect

Palaeogeography, Palaeoclimatology, Palaeoecology

journal homepage: www.elsevier.com/locate/palaeo

Northern high-latitude sea ice variation linked with East Asian monsoon anomalies during the Younger Dryas

Xiaolong Chen [a,b], Hongbin Zhang [b,*], Michael L. Griffiths [c], Xiaogui Peng [a], Liangzhe Yang [a], Ming Yu [a], Junhua Huang [d], Shuyu Xue [b], Hai Cheng [e], Shuai Chen [a]

[a] Hubei Institute of Geosciences, Wuhan 430034, China
[b] State Key Laboratory of Biogeology and Environmental Geology, China University of Geosciences, Wuhan 430074, China
[c] Department of Environmental Science, William Paterson University, Wayne, NJ 07470, USA
[d] State Key Laboratory of Geological Processes and Mineral Resources, China University of Geosciences, Wuhan 430074, China
[e] Institute of Global Environmental Change, Xi'an Jiaotong University, Xi'an 710049, China

ARTICLE INFO

Editor: Dr. Howard Falcon-Lang

Keywords:
Younger Dryas
Asian monsoon
Sea ice
Stalagmite
Seasonality

ABSTRACT

The abrupt weakening of the East Asian summer monsoon (EASM) during Younger Dryas (YD) has been attributed to freshwater discharge into the North Atlantic ocean and resultant Northern Hemisphere cooling. Recent studies have found that sea ice variability in the Nordic Sea during the YD exerted a great influence upon the northern high-latitude climate. However, the influence of sea ice upon EASM evolution during YD event remains unclear. In this paper, we report two precisely-dated speleothem oxygen isotope records from the EASM-dominated region of central China. Our records archive abrupt changes in EASM variability during the YD event. Initially, there was a significant strengthening of the EASM during the mid-YD following the gradually increased Atlantic meridional overturning circulation (AMOC). Later this trend reversed at ~12.15 ka due to northern high-latitude sea ice fluctuations and a consequent reduction of AMOC. At the YD termination, abrupt intensification of the EASM was synchronous with the rapid decline of sea-ice and recovery of the AMOC indicating that sea ice variability was a significant influence on high latitude climate and EASM variation during the YD.

1. Introduction

The Younger Dryas (YD) chronozone, which occurred between ~12,900 and ~ 11,500 year ago, was the latest large-scale climate fluctuation of the deglaciation, and as such has received more attention than any other climate event (Broecker, 2003; Broecker et al., 2010). It has been purported that the YD was triggered by the abrupt flooding of Lake Agassiz into the North Atlantic during the final retreat of the Laurentide Ice Sheet (LIS), which, through disruption to the Atlantic Meridional Overturning Circulation (AMOC), resulted in rapid cooling in the northern high latitudes (Broecker et al., 1989; Condron and Winsor, 2012; Tarasov and Peltier, 2005). Through large-scale reorganizations in atmospheric and oceanic circulation, the YD cold event is widely identified in stalagmite records from both the Asian summer monsoon (ASM) and the Indo-Australia summer monsoon (IASM) domains (Cheng et al., 2020; Liu et al., 2008; Ma et al., 2012; Partin et al., 2015; Sinha et al., 2005; Wang et al., 2022), with the ASM exhibiting a general weakening during the YD and the IASM a general strengthening (Fig. 1).

Recently, some new studies propose that the sea ice variability during YD have great influence upon the northern high latitudes climate (Bakke et al., 2009; Cabedo-Sanz et al., 2013; Pearce et al., 2013). Specifically, an intermittent climate anomaly during the mid-YD event has been documented in high-resolution lake cores (Bakke et al., 2009; Brauer et al., 2008), marine sediments (Elmore and Wright, 2011; McManus et al., 2004; Thornalley et al., 2011) and stalagmite records (Baldini et al., 2015; Bartolomé et al., 2015; Genty et al., 2006) in the northern high-latitude regions, called the "12.15 kyr event", which was attributed to the sea-ice variability and corresponding meridional position of the North Atlantic westerlies. However, the influence of sea ice upon East Asian monsoon evolution during YD event was still unclear.

Here we present two precisely dated stalagmite records from central China, which archive the abrupt changes in EASM variability during the YD event. By comparing our new records with other records from nearby region and northern high latitudes, we observed a gradually strengthened EASM during mid-YD following the gradually increased AMOC.

* Corresponding author.
E-mail address: zhanghb@cug.edu.cn (H. Zhang).

https://doi.org/10.1016/j.palaeo.2023.111702
Received 13 March 2023; Received in revised form 28 June 2023; Accepted 28 June 2023
Available online 29 June 2023

This increasing trend was reversed at ~12 ka due to enhanced northern high-latitude sea ice fluctuations (centered at ~12.15 ka) and the consequent reduction of AMOC.

2. Material and methods

Hailuo Cave (Fig. 1, 109°59′ E, 30°41′ N), located in Hubei Province, along the Yangtze river in central China. Similar to the nearby Heshang Cave (Hu et al., 2008), Hailuo Cave was developed in Lower Cambrian fine crystalline calcareous dolomite strata. The regional climatology is subtropical monsoonal in nature, and is influenced by both the EASM and Indian Summer Monsoon (ISM). During the boreal summer (June to September), the Mei-Yu front of the EASM system, and the associated summer monsoon rain bursts, deliver more than 60% (mean annual is 1200–1300 mm) of the annual precipitation to the site. The mean annual temperature is about 13– 15 °C.

The stalagmites HL6 (26 cm in length) and HL31 (21 cm in length) used in this study were collected from Hailuo Cave in 2013. The HL31 speleothem was broken into two sections during the sampling in field. We only use the lower part of this stalagmite in this study. In total, 11 and 9 subsamples were milled from flat polished surfaces of HL6 and HL31 using a hand-held carbide dental drill (see Table. 1) for the U—Th dating at Xi'an Jiaotong University Isotope Laboratory. The procedure for chemical separation and purification of uranium and thorium follows

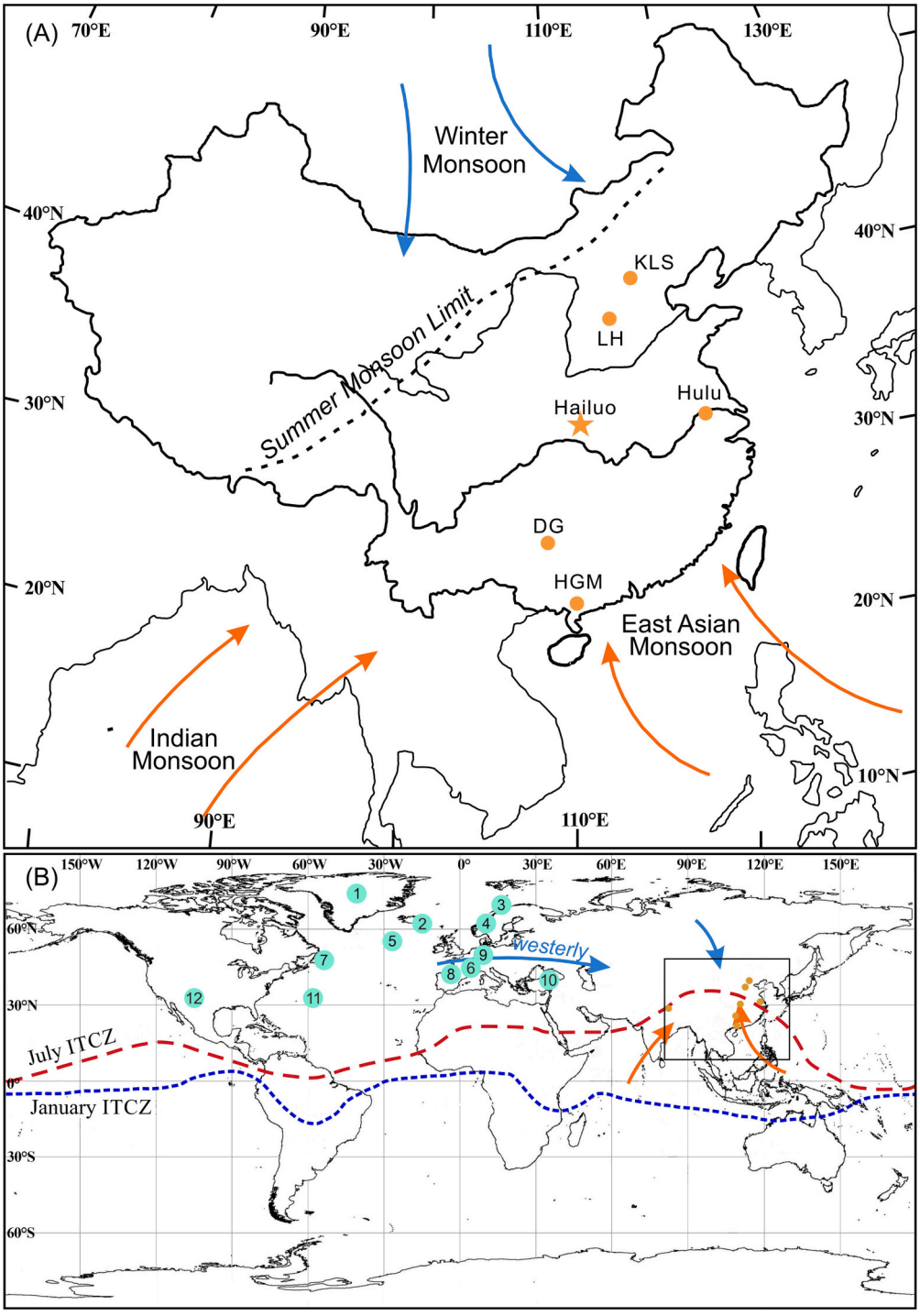

Fig. 1. (A) Location of Hailuo Cave and other sites discussed in the text and modern atmospheric circulation of China. KLS: Kulishu Cave (Ma et al., 2012); LH: Lianhua Cave (Dong et al., 2015); Hulu Cave (Wang et al., 2001); DG: Dongge Cave (Yuan et al., 2004); HGM: Huguang Maar Lake (Yancheva et al., 2007). Arrows indicate the three monsoon systems (East Asian summer monsoon, Indian summer monsoon, and East Asian winter monsoon) which affect annual rainfall in the region. (B) The compared sites in this study: 1-Greenland ice cores: NGRIP (Rasmussen et al., 2006); 2-South Iceland Rise (Thornalley et al., 2011); 3- JM99–1200 core from Andfjorden off northern Norway (Cabedo-Sanz et al., 2013); 4-Lake Kråkenes (Bakke et al., 2009); 5-Core KN166–14 11JPC from Gardar Drift (Elmore and Wright, 2011); 6-Chauvet Cave (Genty et al., 2006); 7-Core AI07-14G from Placentia Bay, Newfoundland (Pearce et al., 2013). 8-La Garma Cave (Baldini et al., 2015) and Seso Cave System (Bartolomé et al., 2015); 9-Lake Meerfelder Maar (Brauer et al., 2008). 10-Sofular Cave (Fleitmann et al., 2009); 11-Bermuda Rise (McManus et al., 2004); 12-Fort Stanton Cave (Asmerom et al., 2010);

Table 1
^{230}Th dating results of HL6 and HL31. The error is 2σ error.

Sample	Depth	^{238}U		^{232}Th		^{230}Th / ^{232}Th		d^{234}U*		^{230}Th / ^{238}U		^{230}Th Age (yr)		^{230}Th Age (yr)		^{230}Th Age (yr BP)		d^{234}U$_{Initial}$**	
Number	mm	(ppb)		(ppt)		(atomic x10^{-6})		(measured)		(activity)		(uncorrected)		(corrected)		(corrected)		(corrected)	
HL6–1	3.5	3203.3	±4.9	68	±4	91,325	±5945	840.2	±2.4	0.1171	±0.0003	7133	±21	**7133**	**±21**	**7070**	**±21**	857	±2
HL6–2	18.5	364.0	±0.3	85	±4	8968	±433	875.7	±2.1	0.1273	±0.0009	7622	±59	**7619**	**±59**	**7556**	**±59**	895	±2
HL6–3	24	656.9	±0.6	35	±3	41,997	±4191	859.5	±2.1	0.1356	±0.0005	8213	±36	**8212**	**±36**	**8149**	**±36**	880	±2
HL6–4	48	1007.9	±1.0	44	±3	53,921	±3401	902.9	±2.3	0.1425	±0.0004	8440	±28	**8440**	**±28**	**8377**	**±28**	925	±2
HL6–5	90	465.2	±0.5	33	±4	34,241	±3642	926.9	±2.3	0.1492	±0.0008	8734	±47	**8733**	**±47**	**8670**	**±47**	950	±2
HL6–6	120	509.8	±0.5	216	±6	6012	±156	927.6	±2.3	0.1545	±0.0007	9053	±44	**9047**	**±44**	**8984**	**±44**	952	±2
HL6–7	167	3970	±6.3	52	±5	203,755	±20,278	944.5	±2.5	0.1605	±0.0004	9333	±25	**9332**	**±25**	**9269**	**±25**	970	±3
HL6–8	175	979.0	±0.9	376	±8	8200	±177.2	892.4	±2.1	0.1912	±0.0005	11,522	±34	**11,517**	**±34**	**11,454**	**±34**	921.9	±2
HL6–9	232	4003	±7.0	1201	±24	11,240	±227.5	919.9	±2.6	0.2045	±0.0005	12,177	±33	**12,173**	**±33**	**12,110**	**±33**	952	±3
HL6–10	250.5	1265.1	±1.3	303	±7	14,291	±337	916.2	±2.3	0.2075	±0.0005	12,387	±34	**12,383**	**±34**	**12,320**	**±34**	949	±2
HL-6-B	261	5959	±40	593	±12	34,638	±732	923	±5	0.2089	±0.0015	12,430	±100	**12,428**	**±100**	**12,365**	**±100**	956	±6
***HL-31a-B**		2625	±2	570	±12	11,928	±255	851.4	±1.7	0.1569	±0.0003	9596	±19	**9596**	**±19**	**9533**	**±19**	875	±2
HL31–1	7	2087	±3	48	±4	129,636.2	±12,068.1	779.4	±2.2	0.1814	±0.0004	11,638	±33	**11,638**	**±33**	**11,575**	**±33**	805	±2
HL31–2	43	1464	±2	525	±12	8585.6	±206.4	801.0	±2.2	0.1869	±0.0008	11,855	±58	**11,849**	**±58**	**11,785**	**±58**	828	±2
HL31–3	85	4561.5	±9.1	174	±4	85,574	±2147	848.8	±2.4	0.1979	±0.0005	12,242	±37	**12,241**	**±37**	**12,177**	**±37**	879	±3
HL31–4	128	8889.1	±23.4	580	±13	49,455	±1087	801.8	±2.6	0.1956	±0.0006	12,430	±43	**12,429**	**±43**	**12,365**	**±43**	830	±3
HL31–5	164	6339.5	±15.5	519	±12	39,747	±889	749.7	±2.6	0.1974	±0.0006	12,949	±46	**12,947**	**±46**	**12,883**	**±46**	778	±3
HL31–6	235	1967.9	±3.0	294	±7	25,579	±598	898.5	±2.5	0.2318	±0.0006	14,061	±45	**14,059**	**±45**	**13,995**	**±45**	935	±3
HL31–7	280.5	2931	±4	162	±5	69,771.9	±2068.6	879.9	±2.5	0.2339	±0.0005	14,343	±39	**14,343**	**±39**	**14,279**	**±39**	916	±3
HL31–8	311	559.6	±0.6	475	±11	4508	±103	849.4	±2.4	0.2321	±0.0009	14,476	±62	**14,463**	**±63**	**14,400**	**±63**	885	±2

U decay constants: $\lambda_{238} = 1.55125 \times 10^{-10}$ (Jaffey et al., 1971) and $\lambda_{234} = 2.82206 \times 10^{-6}$ (Cheng et al., 2013). Th decay constant: $\lambda_{230} = 9.1705 \times 10^{-6}$ (Cheng et al., 2013). The error is 2σ error.
*$\delta^{234}U = ([^{234}U/^{238}U]_{activity} - 1) \times 1000$. ** $\delta^{234}U_{initial}$ was calculated based on ^{230}Th age (T), i.e., $\delta^{234}U_{initial} = \delta^{234}U_{measured} \times e^{\lambda 234 \times T}$. Corrected ^{230}Th ages assume the initial $^{230}Th/^{232}Th$ atomic ratio of $4.4 \pm 2.2 \times 10^{-6}$. Those are the values for a material at secular equilibrium, with the bulk earth $^{232}Th/^{238}U$ value of 3.8. The errors are arbitrarily assumed to be 50%. B.P. stands for "Before Present" where the "Present" is defined as the year 1950 CE.

* **HL-31a-B was the bottom date of upper part of the HL31 speleothem.**

the method that described in Edwards et al. (1987) and Cheng et al. (2000). Uranium and thorium isotopes measurements were performed on a multi-collector inductively coupled plasma mass spectrometer (MC-ICPMS, Thermo-Finnigan Neptune), following protocols of Cheng et al. (2013).

Stable oxygen and carbon isotope were analyzed at the State Key Laboratory of Geological Processes and Mineral Resources, China University of Geosciences, Wuhan. In total, 260 and 210 subsamples were drilled continuously along the extension axis of the stalagmites HL6 and HL31 at 1 mm increments. The measurements were conducted on a Thermo-Finnigan MAT-253 isotope ratio mass spectrometer with an online, automated carbonate preparation system (Kiel IV). Values are reported in per mil (‰) relative to Vienna Peedee Belemnite (VPDB) standard. Duplicate measurements of National standards GBW04416 (TB-1) and GBW04417 (TB-2), along with a laboratory internal standard ISTB-1, show a long-term reproducibility of ~0.06‰ for $\delta^{18}O$ and ~0.03‰ for $\delta^{13}C$ (1σ).

3. Results and discussion

3.1. Chronology

The uranium and thorium isotopic compositions and ^{230}Th ages for stalagmite HL6 and HL31 are presented in Table 1. HL6 and HL31 have relative high uranium concentration, with ^{238}U ranging from 360 to 8800 ppb. The ^{232}Th concentration is much lower, ranging from 33 to 1201 ppt. All the ^{230}Th dates from two speleothem are in stratigraphic order. Two hiatus intervals were found in HL6 during 11.45 to 9.27 ka and 8.15 to 7.56 ka, and one obvious hiatus on the top of HL31 during 11.5 to 9.5 ka. Age models for $\delta^{18}O$ isotope sequences were constructed using 'StalAge' algorithm (Scholz and Hoffmann, 2011) (Fig. 2).

3.2. Replication test and the interpretation of speleothem $\delta^{18}O$ in EASM

The HL6 and HL31 $\delta^{18}O$ isotope sequences show good agreement with the published speleothem $\delta^{18}O$ records from Asian monsoon domains (Dong et al., 2015; Yuan et al., 2004). Two $\delta^{18}O$ records show coherent periods of isotopic enrichment that are synchronous with pulses of abrupt freshwater flux (Fig. 3A, Liu et al., 2014) and associated desalinization of the Labrador Sea (Solignac et al., 2004), along with abrupt cooling in Greenland recorded in ice cores (Rasmussen et al., 2006) corresponding to the YD and 8.2 ka events. Therefore, following theoretical and empirical studies (Cheng et al., 2016; Liu et al., 2014), here we interpret the speleothem $\delta^{18}O$ changes in Hailuo cave as robust indicators of the EASM monsoon winds on millennial timescales, with depleted (enriched) $\delta^{18}O$ corresponding with strong (weak) East Asian

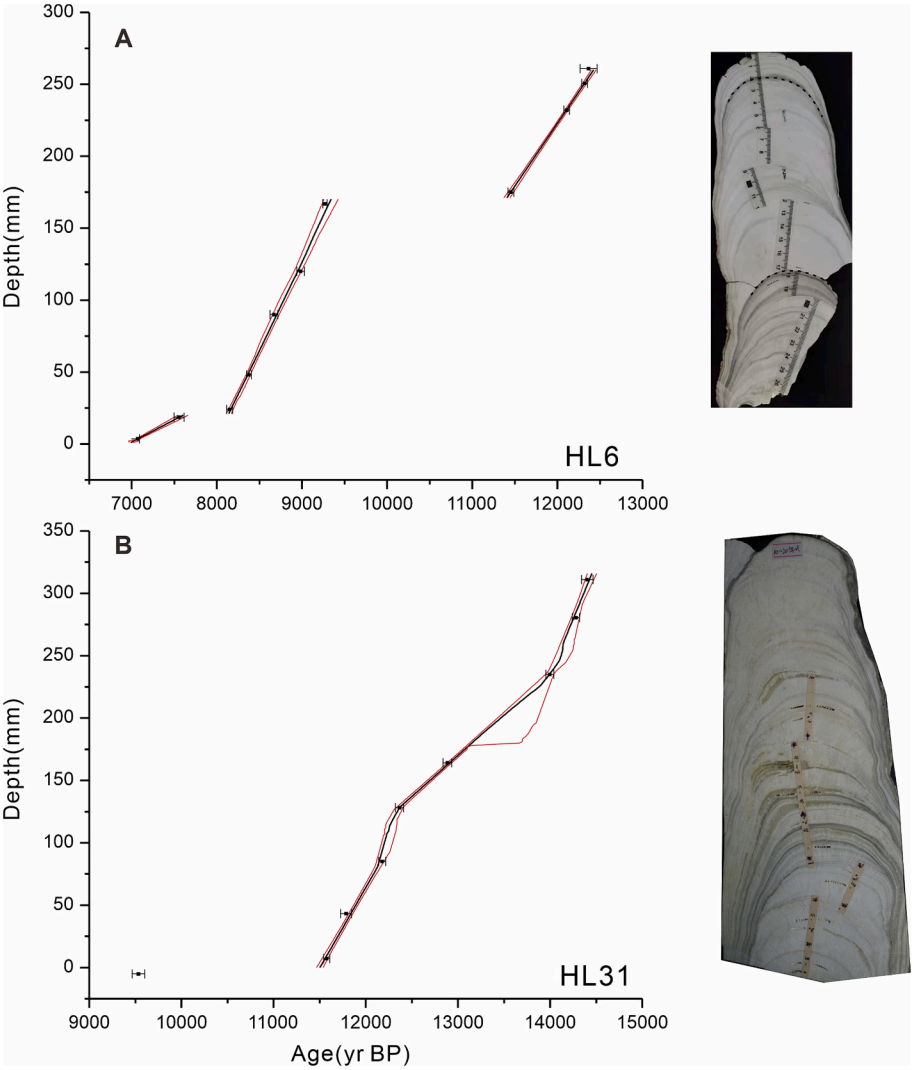

Fig. 2. The scanned sample pictures and the 'StalAge' age model used to construct the $\delta^{18}O$ time series of HL6 and HL31. The red lines indicate the corresponding 2σ uncertainty limits constructed from StalAge. The raw U—Th dates and corresponding 2σ uncertainties are indicated by the black squares and lines. (For interpretation of the references to colour in this figure legend, the reader is referred to the web version of this article.)

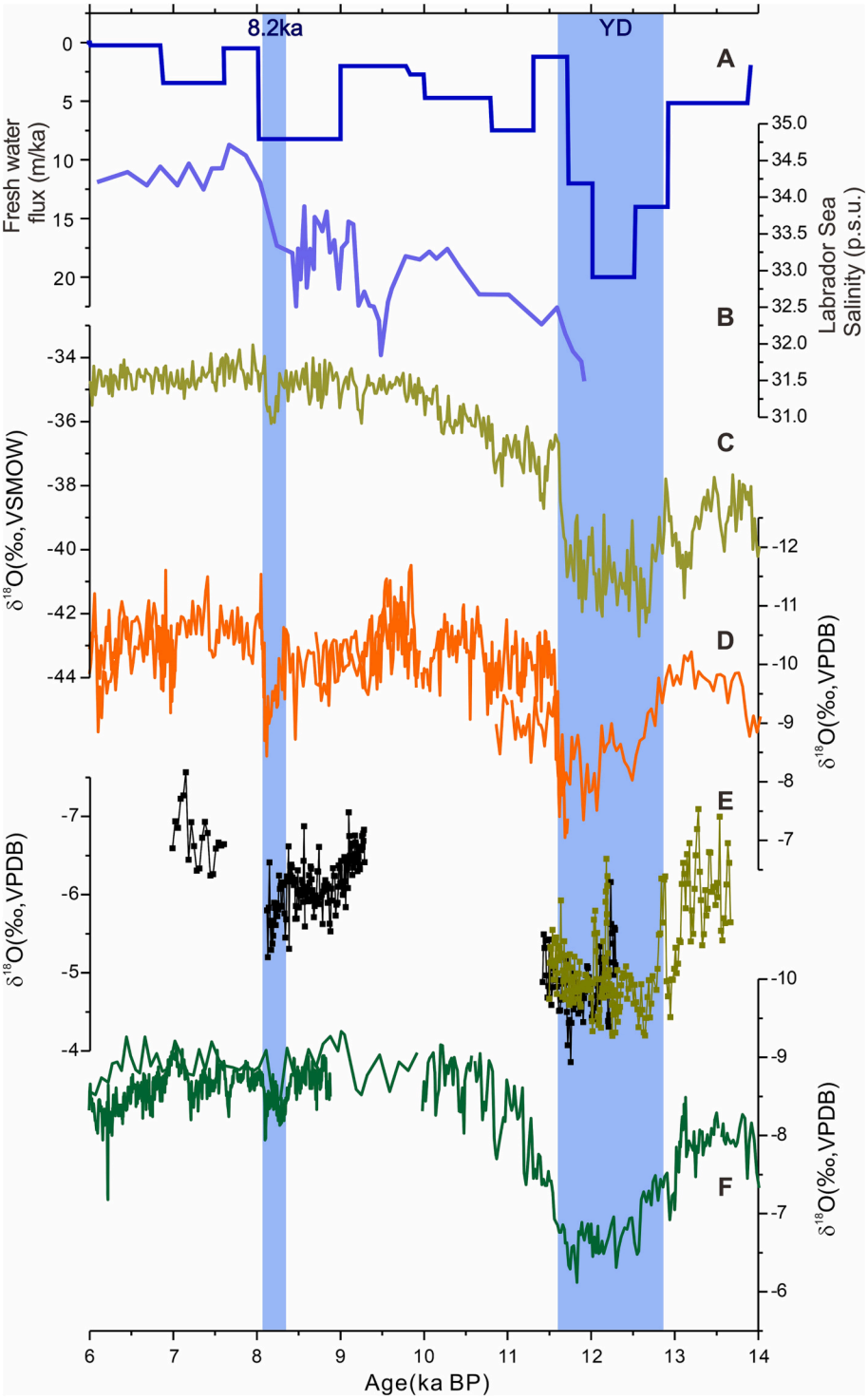

Fig. 3. Comparison of speleothem $\delta^{18}O$ records from the East Asian monsoon region (C) Synthesized meltwater flux in the Northern Hemisphere (Liu et al., 2014); (B) Dinocyst-assemblage salinity estimates from central Labrador Sea, high/low salinity corresponding to strong/weak AMOC (Solignac et al., 2004); (C) Greenland NGRIP ice core $\delta^{18}O$ records (Rasmussen et al., 2006); (D—F) Speleothem $\delta^{18}O$ records from Lianhua Cave (Dong et al., 2015), Hailuo Cave (this study) and Dongge Cave (Dykoski et al., 2005).

southerly winds. During the YD and 8.2 ka events, large-scale northern hemisphere cooling increased the equator-to-pole temperature gradients, causing a reorganization of the Hadley circulation with a southward shift of the ascending branch—the intertropical convergence zone (ITCZ) —which in turn led to anomalous southward cross-equatorial flow and weakening of the Asian summer monsoon (Liu et al., 2014; Cheng et al., 2016).

3.3. Middle Younger Dryas climate anomalies in the EASM domain

In Hailuo cave, following the Bølling-Allerød interstadial (B-A)/YD transition, the $\delta^{18}O$ in HL6 and HL31 all show significant depletion from ~12.3–12.0 ka. This pattern was also observed in other records from the EASM domain, characterized by two to three centennial-scale intervals of monsoon intensification (Liu et al., 2013; Ma et al., 2012; Wang et al., 2001), indicating EASM experienced significant strengthening during the mid-YD. Liu et al. (2013) attributed these centennial-scale YD ASM fluctuations to variations in solar activity with a periodicity of

approximately 200 years. Indeed, following the rapid shift into the YD, the influence of fresh meltwater to the ocean gradually decreased, and sea ice gradually retreated in the Nordic sea and North Atlantic, coinciding with a stable climate state in the higher latitudes from 12.7 to 12.3 ka (Fig. 4A and B) (Bakke et al., 2009; Cabedo-Sanz et al., 2013; Pearce et al., 2013). The mid latitudes also began to warm around this time as a result of a resumption in NADW formation (Elmore and Wright, 2011; Thornalley et al., 2011) (Fig. 4C) and increased AMOC from ~12.5–12.1 ka (Fig. 4D) (McManus et al., 2004). Mid-latitude stalagmite records from Europe (Genty et al., 2006) and North America (Asmerom et al., 2010) (Fig. 4E) and northeastern Brazil (Zhang et al., 2021a) all show a near synchronous change which may relate to a northward shift in the ITCZ, which led to a strengthening of the EASM (Fig. 4F).

At approximately 12.1 ka, the EASM quickly returned to a weakened state (similar to that of the early YD) where it remained until the abrupt termination of the YD at ~11.5 ka. This return to reduced monsoon conditions may best be explained by the preceding warming trend in the mid to high latitudes which affected sea-ice formation and subsequent oceanic heat transport. Indeed, from ~12.3 to 12.15 ka the warm North Atlantic Current system began to penetrate more northward, causing a reduction in the formation of seasonal sea ice in the subpolar North Atlantic and thus permitting the westerly jet to migrate northward; the result of this was increased melting of marine and terrestrial ice (Fig. 4) (Bakke et al., 2009; Pearce et al., 2013). This chain-of-events subsequently increased the flux of freshwater to the North Atlantic, which may, to some extent, have reduced the formation of NADW (Thornalley et al., 2011) (Fig. 4C) and thus weakened the AMOC (McManus et al., 2004) (Fig. 4D), pushing the ITCZ to the south. At the YD termination, abrupt intensification of the EASM was synchronous with the rapid decline of sea-ice and quickly recovery of AMOC, indicating sea ice variability has significant influence on both high latitudes climate and EASM variation during YD.

The observed mean-state shift in high-latitude sea-ice formation and subsequent northward shift of the westerly jet at ~12.15 ka is also synchronous with an abrupt decrease in the dust flux to Greenland (Fig. 5A-C)(Bakke et al., 2009; Brauer et al., 2008; Mayewski et al., 1997), and warmer, more humid winter conditions in western/central Europe (Fig. 5D and E) (Fleitmann et al., 2009; Genty et al., 2006); these patterns were also recently highlighted in a stalagmite record from Seso Cave in the Central Pyrenees (Bartolomé et al., 2015). Coeval with these high latitude changes, the East Asian winter monsoon (EAWM) gradually weakened at ~12 ka (Yancheva et al., 2007), with the stepwise weakening in excellent agreement with European winter climate change, but again quite different from the EASM which remains in a relatively weak state until the late YD (~11.5 ka). Thus, in addition to shifts in the ITCZ due to oceanic heat transport, the higher East Asian speleothem $\delta^{18}O$ through the late YD may also be attributed to changes in seasonality (i.e. weaker seasonality after ~12.1 ka), with warmer winters during the late YD bringing more enriched $\delta^{18}O$ of moisture to the region (Baker et al., 2015; Fig. 5). This change in seasonality may best be explained by changes in the subpolar sea ice distribution during the late YD, which modulated the position of the westerly jet and Siberia High and thus affected European winter climate and the EAWM during the YD.

3.4. Drier interval following the termination of YD event

In HL6 and HL31, a hiatus in growth occurred following the abrupt termination of the YD event around 11. 5 ka to 9.5 ka. Nearby hydroclimate reconstructions from Haozhu Cave speleothem trace element ratios (Fig. 6; Zhang et al., 2018) and Hopanoid records from Dajiuhu peatland (Xie et al., 2013) also suggest drier conditions between 11.5 ka and 10.5 ka. Regarding the latter from Dajiuhu peatland, hopanoids are mainly biosynthesized by aerobic bacteria such that hopanoid concentrations serve as a proxy for water-table depth, i.e., high-hopanoid

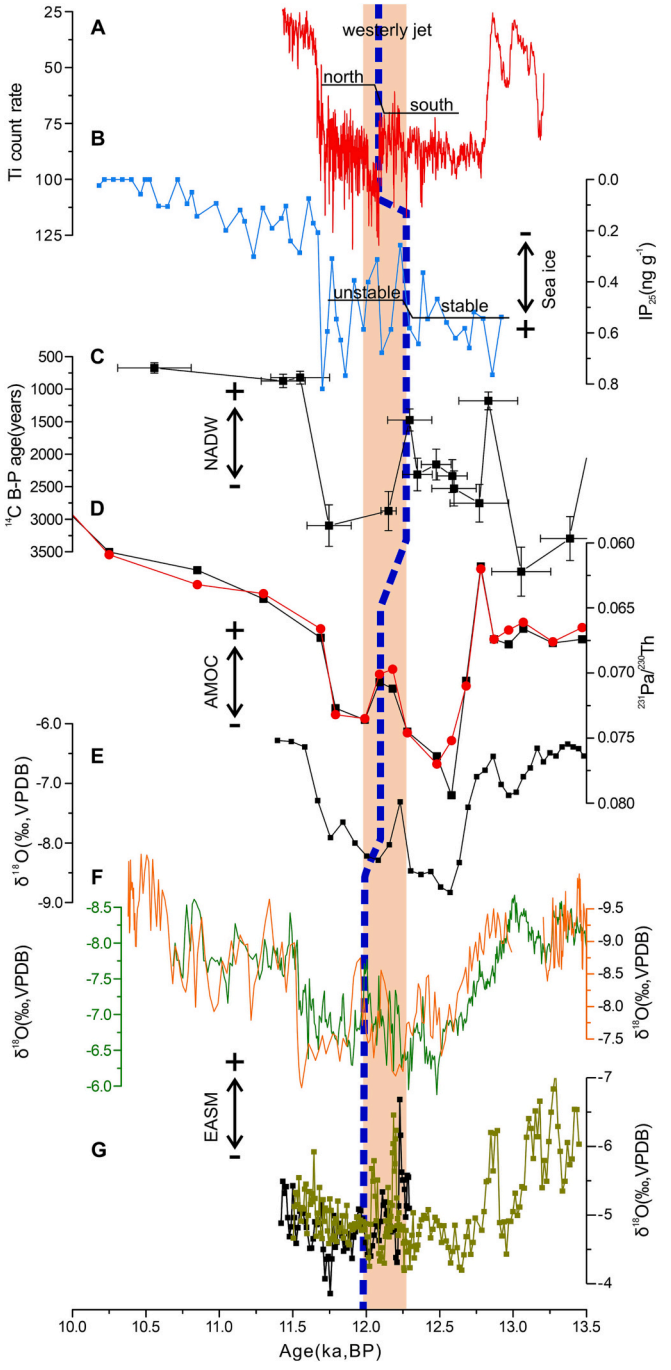

Fig. 4. Mid-YD EASM fluctuation and abrupt YD termination. (A) Ti count rate in Lake Kråkenes reflects changes in the sea ice state and the position of North Atlantic westerlies (Bakke et al., 2009); (B) Sea-ice biomarker IP25 in Core AI07-14G from Placentia Bay, Newfoundland (Pearce et al., 2013); (C) Southern Iceland ventilation age expressed by benthic-planktonic foraminifera ^{14}C age difference (Thornalley et al., 2011); (D) AMOC index inferred from $^{231}Pa/^{230}Th$ from core GGC5 from the Bermuda Rise (McManus et al., 2004); (E) $\delta^{18}O$ record from Stanton Cave (winter rainfall proxy in the Southwest USA) (Asmerom et al., 2010); (F) $\delta^{18}O$ records from KLS, Hulu (Ma et al., 2012; Wang et al., 2001) and Hailuo caves (G). The pink bar indicates the mid-YD fluctuation whilst the blue dashed line represents the mid-YD climate recovery. (For interpretation of the references to colour in this figure legend, the reader is referred to the web version of this article.)

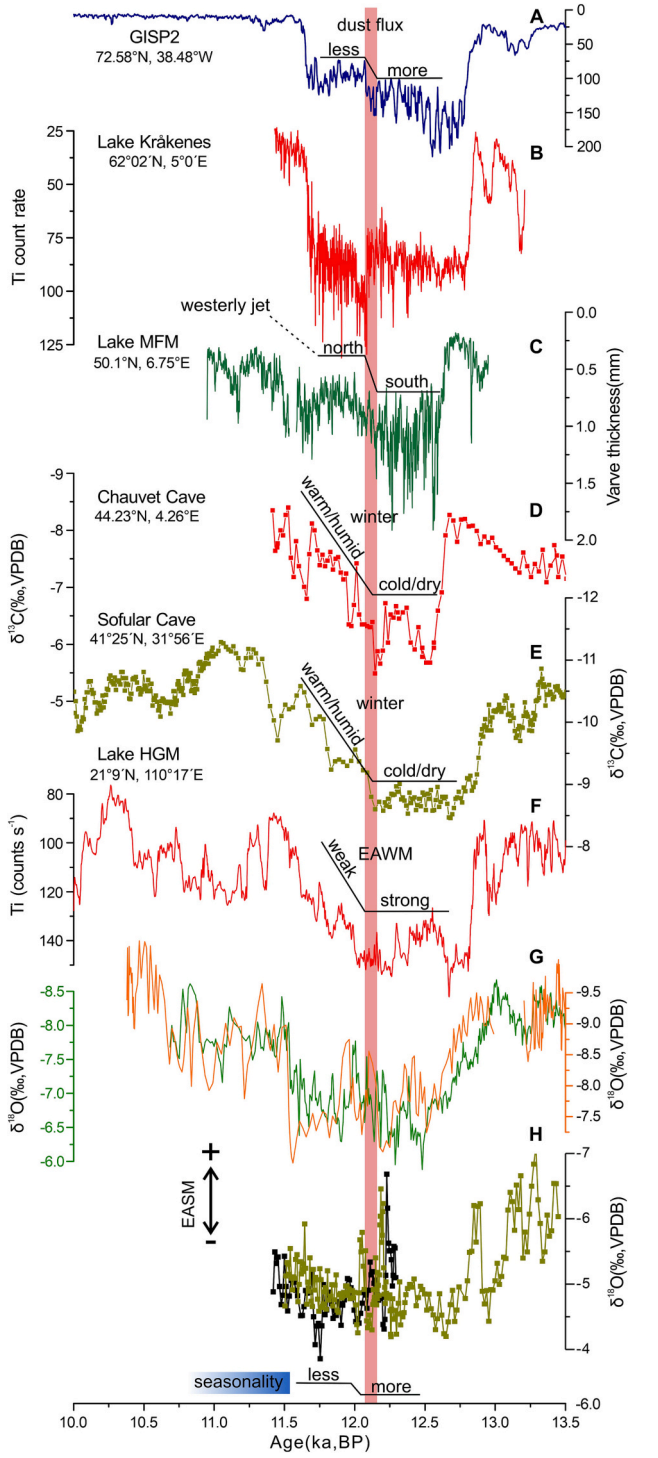

Fig. 5. Correlated seasonality change following the sea-ice fluctuation during the mid-YD. (A) Ca concentration in the GISP2 ice core, dust flux index (Mayewski et al., 1997); (B) Ti counts record from Lake Kråkenes (Bakke et al., 2009) and (C) Varve thickness from Lake Meerfelder Maar (Brauer et al., 2008), indicating the westerly jet shift from south to north at about 12.15 ka; (D-E) Stalagmite $\delta^{13}C$ records from Chauvet Cave, France (Genty et al., 2006) and Sofular Cave, Turkey (Fleitmann et al., 2009); (F) EAWM referred the Ti counts record from Lake Huguang Maar (Yancheva et al., 2007); (G) $\delta^{18}O$ records from KLS, Hulu (Ma et al., 2012; Wang et al., 2001) and Hailuo caves (H). The red bar highlights the '12.15 kyr event' as recorded in northern high latitudes (Bakke et al., 2009). (For interpretation of the references to colour in this figure legend, the reader is referred to the web version of this article.)

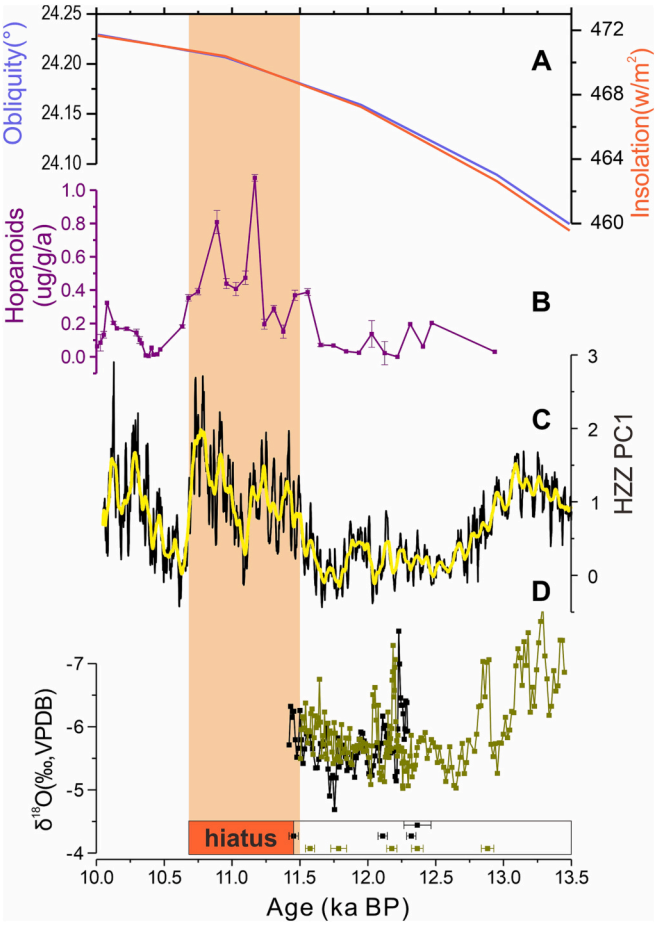

Fig. 6. Drier interval following the termination of YD event. (A) The 21 July insolation at 65°N and the obliquity (Berger, 1978); (B) Hopanoid flux records from Dajiuhu peatland (Xie et al., 2013); (C) Speleothem multiproxy reconstructed hydroclimate from Haozhu Cave (Zhang et al., 2018); (D) $\delta^{18}O$ records from Hailuo caves and the ^{230}Th dates.

abundances are indicative of a deeper water table and aerobic conditions. Given this overwhelming evidence for regional drying, we propose that the hiatus observed in HL6 and HL31 represents a drier interval in central China following the termination of the YD event. Meanwhile, some recent data-model comparison studies from the monsoonal eastern China also suggest a drying climate pattern in central China during the early Holocene (Kong et al., 2017; Zhang et al., 2021b). We thus argue that during the early Holocene, when the impacts of North Atlantic freshwater forcing had subsided, a lower precession and higher obliquity led to increased warmth in the northern high latitudes, and a decreased equator-to-pole temperature gradient that resulted in a northward shifted westerly jet. A result of this sequence-of-events was a shorter Meiyu season which contributed to overall drier conditions in central China (Chiang et al., 2017; Zhang et al., 2018).

4. Conclusion

The abrupt weakening of the EASM during the Younger Dryas climate anomaly has been attributed to a southward shift in the ITCZ due to an abrupt freshwater discharge into the North Atlantic and resultant NH cooling during the final stages of Laurentide Ice Sheet retreat. In this study, using two precisely dated speleothem oxygen-isotope records form central China, we show significant EASM strengthening during the mid-YD, which gradually followed an abrupt increase in AMOC. This increasing trend in the EASM was interrupted at ~12.1 ka due to northern high-latitude sea ice fluctuations (centered at ~12.15 ka) and

the consequent reduction of AMOC. At the YD termination, an abrupt intensification of the EASM was synchronous with the rapid decline of sea-ice and quickly recovery of AMOC, indicating sea ice variability has significant influence EASM variation during YD.

Declaration of Competing Interest

All authors declare no conflict of interest.

Data availability

The original data have been attached in the supplementary material.

Acknowledgement

This work was supported by the Chinese National Natural Science Foundation (grants 42272220, 41902188 and U20A2094) and the 2021 Annual Science and Technology Project of Hubei Geological Bureau (KJ2021-22). This work was supported by a National Science Foundation Paleo Perspectives on Climate Change Award (Award Number 1805544) to Michael L. Griffiths.

Appendix A. Supplementary data

Supplementary data to this article can be found online at https://doi.org/10.1016/j.palaeo.2023.111702.

References

Asmerom, Y., Polyak, V.J., Burns, S.J., 2010. Variable winter moisture in the southwestern United States linked to rapid glacial climate shifts. Nat. Geosci. 3, 114–117.
Bakke, J., Lie, Ø., Heegaard, E., Dokken, T., Haug, G.H., Birks, H.H., Dulski, P., Nilsen, T., 2009. Rapid oceanic and atmospheric changes during the Younger Dryas cold period. Nat. Geosci. 2, 202–205.
Baker, A.J., Sodemann, H., Baldini, J.U.L., Breitenbach, S.F.M., Johnson, K.R., van Hunen, J., Zhang, P., 2015. Seasonality of westerly moisture transport in the East Asian summer monsoon and its implications for interpreting precipitation δ18O. J. Geophys.Res.Atmos. 120, 5850–5862.
Baldini, L.M., McDermott, F., Baldini, J.U.L., Arias, P., Cueto, M., Fairchild, I.J., Hoffmann, D.L., Mattey, D.P., Müller, W., Nita, D.C., Ontañón, R., Garciá-Moncó, C., Richards, D.A., 2015. Regional temperature, atmospheric circulation, and sea-ice variability within the Younger Dryas Event constrained using a speleothem from northern Iberia. Earth Planet. Sci. Lett. 419, 101–110.
Bartolomé, M., Moreno, A., Sancho, C., Stoll, H.M., Cacho, I., Spötl, C., Belmonte, Á., Edwards, R.L., Cheng, H., Hellstrom, J.C., 2015. Hydrological change in Southern Europe responding to increasing North Atlantic overturning during Greenland Stadial 1. Proc. Nat. Acad. Sci. 112, 6568–6572.
Berger, A., 1978. Long-term variations of daily insolation and Quaternary climatic changes. J. Atmos. Sci. 35, 2362–2367.
Brauer, A., Haug, G.H., Dulski, P., Sigman, D.M., Negendank, J.F.W., 2008. An abrupt wind shift in western Europe at the onset of the Younger Dryas cold period. Nat. Geosci. 1, 520–523.
Broecker, W.S., 2003. Does the trigger for abrupt climate change reside in the ocean or in the atmosphere? Science 300, 1519–1522.
Broecker, W.S., Denton, G.H., Edwards, R.L., Cheng, H., Alley, R.B., Putnam, A.E., 2010. Putting the Younger Dryas cold event into context. Quat. Sci. Rev. 29, 1078–1081.
Broecker, W.S., Kennett, J.P., Flower, B.P., Teller, J.T., Trumbore, S., Bonani, G., Wolfli, W., 1989. Routing of meltwater from the laurentide ice-sheet during the younger dryas cold episode. Nature 341, 318–321.
Cabedo-Sanz, P., Belt, S.T., Knies, J., Husum, K., 2013. Identification of contrasting seasonal sea ice conditions during the Younger Dryas. Quat. Sci. Rev. 79, 74–86.
Cheng, H., Edwards, R.L., Hoff, J., Gallup, C.D., Richards, D.A., Asmerom, Y., 2000. The half-lives of uranium-234 and thorium-230. Chem. Geol. 169, 17–33.
Cheng, H., Edwards, R.L., Shen, C.C., Polyak, V.J., Asmerom, Y., Woodhead, J., Hellstrom, J., Wang, Y.J., Kong, X.G., Spotl, C., Wang, X.F., Alexander, E.C., 2013. Improvements in Th-230 dating, Th-230 and U-234 half-life values, and U-Th isotopic measurements by multi-collector inductively coupled plasma mass spectrometry. Earth Planet. Sci. Lett. 371, 82–91.
Cheng, H., Edwards, R.L., Sinha, A., Spötl, C., Yi, L., Chen, S., Kelly, M., Kathayat, G., Wang, X., Li, X., Kong, X., Wang, Y., Ning, Y., Zhang, H., 2016. The Asian monsoon over the past 640,000 years and ice age terminations. Nature 534, 640–646.
Cheng, H., Zhang, H., Spötl, C., Baker, J., Sinha, A., Li, H., Bartolomé, M., Moreno, A., Kathayat, G., Zhao, J., 2020. Timing and structure of the Younger Dryas event and its underlying climate dynamics. Proc. Nat. Acad. Sci. 117, 23408–23417.
Chiang, J.C.H., Swenson, L.M., Kong, W., 2017. Role of seasonal transitions and the westerlies in the interannual variability of the East Asian summer monsoon precipitation. Geophys. Res. Lett. 44, 3788–3795.
Condron, A., Winsor, P., 2012. Meltwater routing and the Younger Dryas. Proc. Nat. Acad. Sci. 109, 19928–19933.
Dong, J., Shen, C.-C., Kong, X., Wang, H.-C., Jiang, X., 2015. Reconciliation of hydroclimate sequences from the Chinese Loess Plateau and low-latitude East Asian Summer Monsoon regions over the past 14,500years. Palaeogeogr. Palaeoclimatol. Palaeoecol. 435, 127–135.
Dykoski, C.A., Edwards, R.L., Cheng, H., Yuan, D.X., Cai, Y.J., Zhang, M.L., Lin, Y.S., Qing, J.M., An, Z.S., Revenaugh, J., 2005. A high-resolution, absolute-dated Holocene and deglacial Asian monsoon record from Dongge Cave, China. Earth Planet. Sci. Lett. 233, 71–86.
Edwards, R.L., Chen, J., Ku, T.-L., Wasserburg, G., 1987. Precise timing of the last interglacial period from mass spectrometric determination of thorium-230 in corals. Science 236, 1547–1553.
Elmore, A.C., Wright, J.D., 2011. North Atlantic Deep Water and climate variability during the Younger Dryas cold period. Geology 39, 107–110.
Fleitmann, D., Cheng, H., Badertscher, S., Edwards, R.L., Mudelsee, M., Goektuerk, O.M., Fankhauser, A., Pickering, R., Raible, C.C., Matter, A., Kramers, J., Tuysuz, O., 2009. Timing and climatic impact of Greenland interstadials recorded in stalagmites from northern Turkey. Geophys. Res. Lett. 36, L19707.
Genty, D., Blamart, D., Ghaleb, B., Plagnes, V., Causse, C., Bakalowicz, M., Zouari, K., Chkir, N., Hellstrom, J., Wainer, K., 2006. Timing and dynamics of the last deglaciation from European and North african δ13C stalagmite profiles—comparison with Chinese and South Hemisphere stalagmites. Quat. Sci. Rev. 25, 2118–2142.
Hu, C.Y., Henderson, G.M., Huang, J.H., Xie, S., Sun, Y., Johnson, K.R., 2008. Quantification of Holocene Asian monsoon rainfall from spatially separated cave records. Earth Planet. Sci. Lett. 266, 221–232.
Jaffey, A., Flynn, K., Glendenin, L., Bentley, W.t., Essling, A., 1971. Precision measurement of half-lives and specific activities of U 235 and U 238. Phys. Rev. C 4, 1889–1906.
Kong, W., Swenson, L.M., Chiang, J.C., 2017. Seasonal transitions and the westerly jet in the Holocene East Asian summer monsoon. J. Clim. 30, 3343–3365.
Liu, D., Wang, Y., Cheng, H., Kong, X., Chen, S., 2013. Centennial-scale Asian monsoon variability during the mid-Younger Dryas from Qingtian Cave, Central China. Quat. Res. 80, 199–206.
Liu, D.B., Wang, Y.J., Cheng, H., Edwards, R.L., Kong, X.G., Wang, X.F., Wu, J.Y., Chen, S.T., 2008. A detailed comparison of Asian Monsoon intensity and Greenland temperature during the Allerod and Younger Dryas events. Earth Planet. Sci. Lett. 272, 691–697.
Liu, Z.Y., Wen, X.Y., Brady, E.C., Otto-Bliesner, B., Yu, G., Lu, H.Y., Cheng, H., Wang, Y. J., Zheng, W.P., Ding, Y.H., Edwards, R.L., Cheng, J., Liu, W., Yang, H., 2014. Chinese cave records and the East Asia Summer Monsoon. Quat. Sci. Rev. 83, 115–128.
Ma, Z.-B., Cheng, H., Tan, M., Edwards, R.L., Li, H.-C., You, C.-F., Duan, W.-H., Wang, X., Kelly, M.J., 2012. Timing and structure of the Younger Dryas event in northern China. Quat. Sci. Rev. 41, 83–93.
Mayewski, P.A., Meeker, L.D., Twickler, M.S., Whitlow, S., Yang, Q., Lyons, W.B., Prentice, M., 1997. Major features and forcing of high-latitude northern hemisphere atmospheric circulation using a 110,000-year-long glaciochemical series. J.Geophys. Res.Oceans 102, 26345–26366.
McManus, J., Francois, R., Gherardi, J.-M., Keigwin, L., Brown-Leger, S., 2004. Collapse and rapid resumption of Atlantic meridional circulation linked to deglacial climate changes. Nature 428, 834–837.
Partin, J.W., Quinn, T.M., Shen, C.C., Okumura, Y., Cardenas, M.B., Siringan, F.P., Banner, J.L., Lin, K., Hu, H.M., Taylor, F.W., 2015. Gradual onset and recovery of the Younger Dryas abrupt climate event in the tropics. Nat. Commun. 6, 8061.
Pearce, C., Seidenkrantz, M.-S., Kuijpers, A., Massé, G., Reynisson, N.F., Kristiansen, S. M., 2013. Ocean lead at the termination of the Younger Dryas cold spell. Nat. Commun. 4, 1664.
Rasmussen, S.O., Andersen, K.K., Svensson, A., Steffensen, J.P., Vinther, B.M., Clausen, H.B., Siggaard-Andersen, M.L., Johnsen, S.J., Larsen, L.B., Dahl-Jensen, D., 2006. A new Greenland ice core chronology for the last glacial termination. J. Geophys.Res.Atmos. 111, D06102.
Scholz, D., Hoffmann, D.L., 2011. StalAge – an algorithm designed for construction of speleothem age models. Quat. Geochronol. 6, 369–382.
Sinha, A., Cannariato, K.G., Stott, L.D., Li, H.C., You, C.F., Cheng, H., Edwards, R.L., Singh, I.B., 2005. Variability of Southwest Indian summer monsoon precipitation during the Boiling-Allerod. Geology 33, 813–816.
Solignac, S., de Vernal, A., Hillaire-Marcel, C., 2004. Holocene Sea-surface conditions in the North Atlantic—contrasted trends and regimes in the western and eastern sectors (Labrador Sea vs. Iceland Basin). Quat. Sci. Rev. 23, 319–334.
Tarasov, L., Peltier, W., 2005. Arctic freshwater forcing of the Younger Dryas cold reversal. Nature 435, 662–665.
Thornalley, D.J., Barker, S., Broecker, W.S., Elderfield, H., McCave, I.N., 2011. The deglacial evolution of North Atlantic deep convection. Science 331, 202–205.
Wang, Y.J., Cheng, H., Edwards, R.L., An, Z.S., Wu, J.Y., Shen, C.C., Dorale, J.A., 2001. A high-resolution absolute-dated late Pleistocene monsoon record from Hulu Cave, China. Science 294, 2345–2348.
Wang, Z., Chen, S., Wang, Y., Zhao, K., Liang, Y., Cheng, H., Shao, Q., Wang, X., Zhang, J., Wang, Q., 2022. A high-resolution stalagmite record from Luoshui Cave, Central China over the past 23.5 kyr. Quat. Sci. Rev. 282, 107443.
Xie, S.C., Evershed, R.P., Huang, X.Y., Zhu, Z.M., Pancost, R.D., Meyers, P.A., Gong, L.F., Hu, C.Y., Huang, J.H., Zhang, S.H., Gu, Y.S., Zhu, J.Y., 2013. Concordant monsoon-

driven postglacial hydrological changes in peat and stalagmite records and their impacts on prehistoric cultures in Central China. Geology 41, 827–830.
Yancheva, G., Nowaczyk, N.R., Mingram, J., Dulski, P., Schettler, G., Negendank, J.F.W., Liu, J.Q., Sigman, D.M., Peterson, L.C., Haug, G.H., 2007. Influence of the intertropical convergence zone on the East Asian monsoon. Nature 445, 74–77.
Yuan, D.X., Cheng, H., Edwards, R.L., Dykoski, C.A., Kelly, M.J., Zhang, M.L., Qing, J.M., Lin, Y.S., Wang, Y.J., Wu, J.Y., Dorale, J.A., An, Z.S., Cai, Y.J., 2004. Timing, duration, and transitions of the last Interglacial Asian Monsoon. Science 304, 575–578.
Zhang, H.B., Griffiths, M.L., Chiang, J.C.H., Kong, W.W., Wu, S.T., Atwood, A., Huang, J. H., Cheng, H., Ning, Y.F., Xie, S.C., 2018. East Asian hydroclimate modulated by the position of the westerlies during termination I. Science 362, 580–583.
Zhang, H., Cheng, H., Spötl, C., Zhang, X., Cruz, F.W., Sinha, A., Auler, A.S., Stríkis, N.M., Wang, X., Kathayat, G.J.G.R.L., 2021. Gradual South-North climate transition in the Atlantic Realm within the Younger Dryas. Geophys. Res. Lett. 48 e2021GL092620.
Zhang, H., Zhang, X., Cai, Y., Sinha, A., Spoetl, C., Baker, J., Kathayat, G., Liu, Z., Tian, Y., Lu, J., 2021. A data-model comparison pinpoints Holocene spatiotemporal pattern of East Asian summer monsoon. Quat. Sci. Rev. 261, 106911.